ADVANCES IN MAGNETOTELLURIC STUDY OF GEOTHERMAL AREAS

Viacheslav Spichak (Geoelectromagnetic Research Center IPE RAS, Troitsk, Russia; v.spichak@ru.net)

3D MT IMAGING GEOTHERMAL RESERVOIR

3-D RESISTIVITY IMAGE OF THE MINAMIKAYABE GEOTHERMAL AREA

The New Energy and Industrial Development Organisation (NEDO) has conducted geologic, gravity, geochemical, magnetotelluric, and other surveys in the Minamikayabe area of over 9 km^2 in the southern Hokkaido, Japan, in order to detect and subsequently develop geothermal energy sources. In the immediate vicinity of the wells MK-2 and MK-6, over an area of 1.2 x 1.2 km^2, a high accuracy magnetotelluric survey was performed (Takasugi et a1., 1992) with an electrode separation of 100 m in a frequency range from 0,001 to 20,000 Hz and with one side of the survey area parallel and the other perpendicular to the coast (Fig. 1).

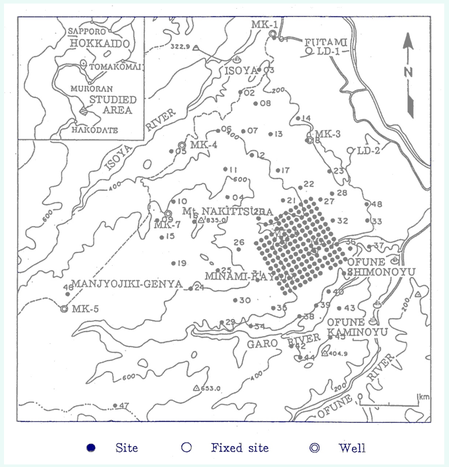

Figure 1. Location scheme of the Minamikayabe survey area (after Takasugi et a1., 1992). Solid dots, MT sounding sites; double circles, wells.

Despite the development of two-dimensional inverse methods, to this day, the approach based on the synthesis of one-dimensional conductivity profiles has remained an effective tool for imaging in the absence of prior information. The necessity of such an approach increases in 3-D case, when the measured data is often deficient, and prior information is too scanty. In this situation, a unique practical recourse, which is especially helpful for a prompt tentative estimation of the resistivity distribution, lies in constructing a 3-D resistivity image of the medium based on the MT fields or their transformations:

$$\tilde{F}_i(\vec{r}\,.(z_{app})_j) = \hat{T}F_i(\vec{r},\omega_j) \quad (j = 1,2,...,N_\omega) \qquad (1)$$

where F_i are the components of the MT field measured on the surface for N_ω frequencies, $\hat{T}$ is the transforming operator, $\tilde{F}$ is the MT field image, $\vec{r}$ is the radius vector of the observation point, j_ω is the frequency, and $(z_{app})_j$ is the apparent depth corresponding to this frequency.
The subsequent Bostick transformation of its frequency dependence into a depth function in fact yields the least screwed image of the three-dimensional geoelectric structure (Fig. 2).

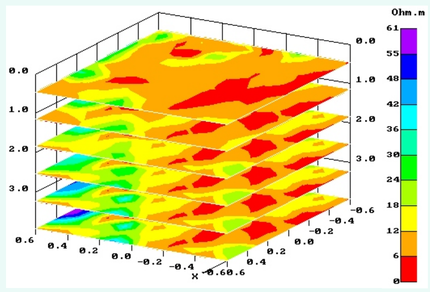

Figure 2. Apparent resistivity ρ_{det} slices.

REFINEMENT OF THE RESISTIVITY IMAGE BY MEANS OF THE BAYESIAN STATISTICAL INVERSION

The resistivity image obtained at the first stage was further refined using Bayesian statistical inversion (Spichak et al., 1999). In the context of this approach, both observations and model parameters (resistivities) are considered as random variables. Bayesian analysis determines the posterior probability density function (PDF) of the resistivity - i.e., the conditional probabilities of the resistivities given the data y, prior information in terms of a resistivity palette $(c_1,...c_L)$, prior PDF q, and the noise level ε:

$$p(\sigma = a/Y = y) = \frac{f(y/a)q(a)}{\sum_{b\in A} f(y/b)q(b)} \qquad (2)$$

where $q(a)$ is the prior probability of the image a and $f(y/a)$ is a conditional probability of the variable $y = (y_{ij}; i = 1,2,...,I; j = 1,2,...,J)$ given the values of the resistivities. It is a function of $a = (a_k; k = 1,2,...,K)$ through $\vec{E}$ and $\vec{H}$ and could be calculated directly as follows:

$$f(y/a) = \prod_{i=1}^{I}\prod_{j=1}^{J} p_{i,j}\left\{y_{i,j} - f\left[\vec{E}\left(M_i,\omega_j,a\right)\vec{H}\left(M_i,\omega_j,a\right)\right]\right\} \qquad (3)$$

where $p_{i,j}$ is the probability density of the noise $\varepsilon_{i,j}$.
The solution of the inverse problem is reduced to the search for the posterior resistivity distribution by means of successive solution of the forward problem for the prior values of the resistivities in all domains of search. The effective algorithm developed basing on this approach (Spichak et al., 1999) enables to construct 3-D geoelectric models by MT data (Spichak, 1999).

In order to construct the 3D resistivity model of the geothermal area full range inversion was carried out taking into account two resistivity logs available in the area (Figs. 3 and 4).

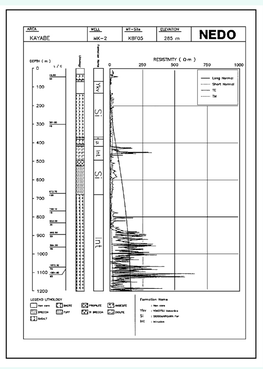

Figure 3. Resistivity logging data from the MK-2 well (Takasugi et al., 1992).

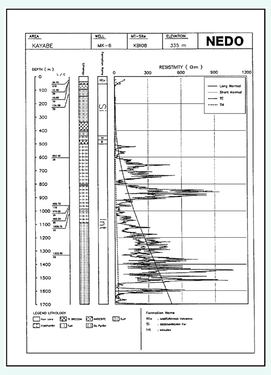

Figure 4. Resistivity logging data from the MK-6 well (Takasugi et al., 1992).

Fig. 5 shows the volume resistivity model of the geothermal area, while Fig. 6 presents highly conductive areas with resistivity values not exceeding 6 Ohm×m, obtained on the basis of the Bayesian inversion taking into account the resistivity profiles from the wells MK-2 and MK-6.

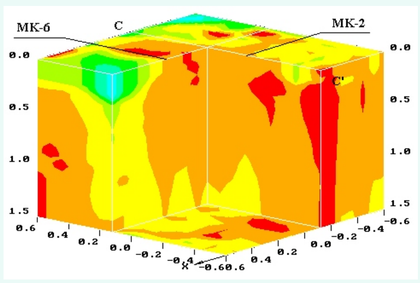

Figure 5. Volume apparent resistivity ρ_{det} map (after Spichak, 2002).

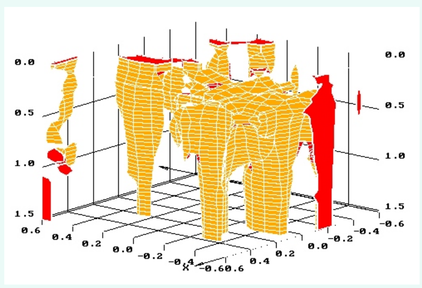

Figure 6. Highly conductive zone (resistivity is less than 6 m) revealed by 3-D inversion of MT data (after Spichak, 2002).

It is easy to see that, firstly, they cluster in the southern part of the zone in question, and, secondly, that their horizontal dimensions at first increase with depth, reaching a maximum in the depth range from about 200 to 800 m, and then decrease again.

CONCLUSIONS

Thus, two-stage inversion of the invariant apparent resistivity data based on rough imaging followed by refinement of the resistivity distribution by means of the Bayesian statistical inversion enabled to re-construct a 3-D geoelectric structure beneath the Minamikayabe region and to delineate a highly conductive zone that can be associated with the geothermal reservoir.

REFERENCES

Spichak, V.V., 1999. Magnetotelluric fields in three-dimensional geoelectric models (in Russian). Scientific World, Moscow, 204pp.

Spichak, V.V., 2001. Three-dimensional interpretation of MT data in volcanic environments (computer simulation). Annali di Geofisica **44** (2), 273-286.

Spichak, V.V., 2002. Advanced three-dimensional interpretation technologies applied to the MT data in the Minamikayabe thermal area (Hokkaido, Japan). Expanded abstr. EAGE 64th Conference, Florence, Italy.

Spichak V.V. 2006. Estimating temperature distributions in geothermal areas using a neuronet approach. Geothermics, **35**, 181-197.

Spichak, V.V., Fukuoka, K., Kobayashi, T., Mogi, T., Popova, I., and Shima, H., 1999. Neural - network based interpretation of insufficient and noisy MT data in terms of the target macro parameters. Expanded abstr. II Symp. on 3D Electromagnetics, Salt Lake city, USA, 297-300.

Spichak, V.V., Menvielle, M., and Roussignol, M., 1999. Three-dimensional inversion of MT data using Bayesian statistics. In: Spies, B., and Oristaglio, M. (Eds.), 3D Electromagnetics, SEG monograph, GD7, Tulsa, USA, 406-417.

Spichak, V.V., and Popova, I.V., 2000. Artificial neural network inversion of MT - data in terms of 3D earth macro parameters. Geoph. J. Int. **42**, 15-26.

Spichak, V.V., Zakharova, O.K., Rybin, A.K., 2006. On the possibility of the indirect electromagnetic geothermometer. Dokl. Russian Akad. Sci. (in Russian) (in press).

Takasugi S., Tanaka K., Kawakami N. and Muramatsu S., 1992. High Spatial Resolution of the Resistivity Structure Revealed by a Dense Network MT Measurement - A Case Study in the Minamikayabe Area, Hokkaido, Japan, Geomag. Geoelectr., **44**, 289-308.

MT SOUNDING OF FAULTS

DETECTION OF THE FAULT MACRO-PARAMETERS

A model class consisting of a dipping fault in the basement of a two-layer earth with the fault in contact with the overburden is used for numerical experiments. Six macroparameters of the 3-D model, namely the thickness of the top layer, coinciding with the depth of the fault (D), the conductivity ratio between the first and second layers ($C1/C2$), the conductivity contrast of the fault (C/C2), and the width (W), length (L) and dip angle of the fault (A)) are used (Fig.7).

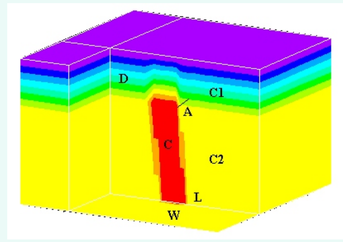

Figure 7. 3D fault model.

Various groups of magnetotelluric field components and their transformations are studied in order to estimate the effect of the data type used on the ANN recognition ability. It is found that use of only xy- and yx-components of impedance phases results in reasonable recognition errors for all unknown parameters (D: 0.02%, $C1/C2$: 8.4 %, C/$C2$: 26.8 %, W: 0.02 %, L: 0.02 %, A: 0.24%).

The influence of the size and shape of the training data pool (including the 'gaps in education' and 'no target' effects) on the recognition properties are studied. Results from numerous ANN tests demonstrate that it possesses good enough interpolation and extrapolation abilities if the training data pool contains a sufficient number of representative data sets.

The effect of noise is estimated by means of mixing the synthetic data with 30, 50 and 100 per cent Gaussian noise. The unusual behavior of the recognition errors for some of the model parameters when the data become more noisy (in particular, the fact that an increase in error is followed by a decrease) indicates that the use of standard techniques of the noise reduction may give an opposite result, so the development of a special noise treatment methodology is required.

Figure 8 demonstrates graphs of the recognition errors for all unknown parameters of the fault model depending on the level of Gaussian noise added to the testing data. It is seen that minima for all curves are attributed to the noise levels in testing data equal to those in the teaching data.

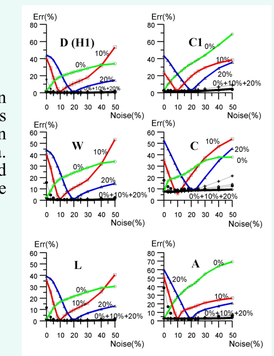

Figure 8. Relative recognition errors for all model parameters depending on the level of Gaussian noise added to the testing data. Numbers (0%, 10%, 20% and 0%+10%+20%) mean the "noise spectrum" in the teaching data.

However, since the level of noise in the real data is not known in advance, it is important to know *how* to mix the teaching data with artificial noise. Spichak et al. (1999) revealed that teaching the ANN by synthetic data mixed with a noise of different levels ranging from 0% (no noise) to some level, which exceeds the maximal one in the data, enables to diminish greatly the recognition errors and results in robust parameters' recognition even if the noise levels in testing and teaching data are different. In other words, prior knowledge about the noise level in the data becomes not necessary. This is demonstrated by the graphs in Figure 9-9 marked as (0%+10%+20%). In this case the recognition errors for all model parameters do not exceed 5-10% even if the level of noise in the testing data reaches 50%.

Thus, it is shown that the ANN-based recognition can be successfully used for inversion if the data correspond to the model class familiar to the ANN. No initial guess regarding the parameters of the 3-D target or 1-D layering is required. The ability of the ANN to teach itself real geophysical (not only electromagnetic) data measured at a given location over a sufficiently long period means that there is the potential to use this approach for interpreting monitoring data.

DETECTION OF THE HYDROTHERMAL FLUID RESISTIVITY VARIATION

Spichak (2001) studied the resolving power of MT data with respect to the variation of the resistivity in the geothermal reservoir depending on the fault presence.

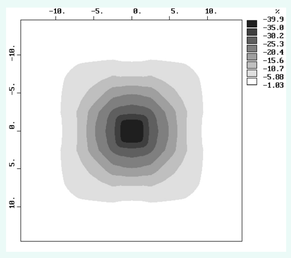

Figure 9. Resistivity variation at the earth's surface due to resistivity variation in the geothermal reservoir.

Matching of a Figure 9 with a Figure 10 shows that the fluid bearing fault strengthens the effect of fluid resistivity variation in the geothermal reservoir approximately by three times. Moreover, it increases the diameter of a zone of reliable monitoring and reduces the period threshold sufficient for detection of even small variations of electric resistivity caused by temperature changes.

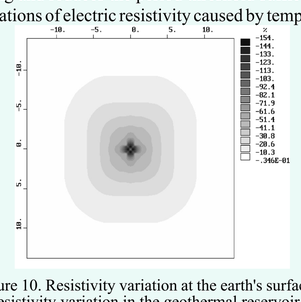

Figure 10. Resistivity variation at the earth's surface due to resistivity variation in the geothermal reservoir in the presence of the fault.

MT GEOTHERMOMETER

Estimation of temperature in the Earth's interior is usually based on the ground heat flow data and assumptions on the vertical temperature gradient. Meanwhile, in geothermal areas characterized by significant fluid migration this approach may fail. Spichak et al. (2006) have developed an alternative way based on incontact temperature estimations using the measurements of magnetotelluric field on the Earth's surface. Basing on the neuronet analysis of MT and temperature data measured at the Bishkek geodynamical test site in the northern Tien Shan (Fig. 11, Fig. 12), a feasibility of indirect electromagnetic geothermometer is substantiated.

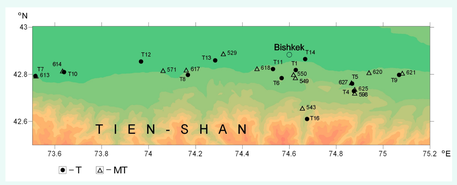

Figure 11. Location scheme of MT sites and wells for which temperature data were available.

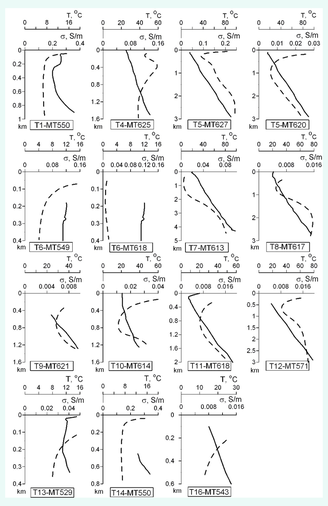

Figure 12. Dependences of the electric conductivity (dashed line) revealed from MT data and temperature (solid line) on the depth.

An optimal technique for MT measurements and involvement of temperature logs available was developed. This technique provides a reduction of the remote temperature estimation errors down to their minimum level. Figure 13 displays variations of relative rms error of the temperature prognosis in the well for the case of only temperature data used (triangles) and for the case of joint use of electromagnetic data together with temperature logs (dots).

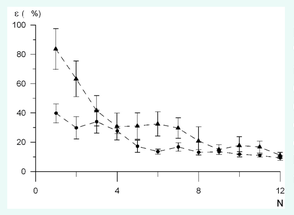

Figure 13. Average relative error ε (in %) of temperature prognosis based on the data about electric conductivity (dots) and about temperature logs (triangles) as a function of the number of pairs (N) of temperature and electric conductivity profiles (or temperature logs only) involved in neuronet training.

An optimal technique for MT measurements and involvement of temperature logs available was developed. This technique provides a reduction of the remote temperature estimation errors down to their minimum level. Figure 13 displays variations of relative rms error of the temperature prognosis in the well for the case of only temperature data used (triangles) and for the case of joint use of electromagnetic data together with temperature logs (dots).

It was shown that the use of 6-8 temperature logs for calibration of electromagnetic data results in 12% relative error of the temperature estimation (Fig. 14), whereas availability of prior geological information about the region under study makes it possible to decrease this error furthermore.

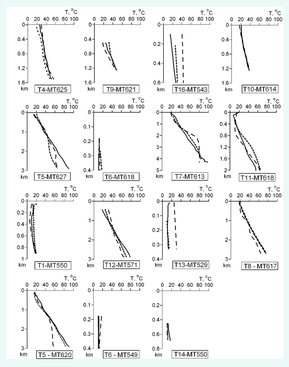

Figure 14. Measured and modeled distributions of temperature in wells. Solid line-measured temperature, dashed line-temperature model based on the temperature data only; line with dots - temperature model based on MT data.

Practical application of this method will enable one, first, to refine the temperature estimates in cases when the amount of temperature logs available is insufficient; second, to perform more precise temperature prediction in extrapolation mode; third, to monitor the well temperature basing on surface observations of MT field and, at last, to carry out contactless remote estimation of temperature in wells in the regions with extreme conditions unsuitable for traditional geothermometers.

CONCLUSIONS

Magnetotelluric sounding of geothermal areas enables:

- 3D imaging geoelectric structure;
- mapping geothermal reservoir;
- detection of the fluid bearing faults;
- monitoring variations of the system macro-parameters;
- indirect estimation of the sub-surface temperature.